

NLO QCD corrections to hadronic Higgs production with heavy quarks

S. Dawson^a, C. B. Jackson^b, L. H. Orr^c, L. Reina^{b*}, D. Wackerroth^d

^aPhysics Department, Brookhaven National Laboratory, Upton, NY 11973-5000, USA

^bPhysics Department, Florida State University, Tallahassee, FL 32306-4350, USA

^cDepartment of Physics and Astronomy, University of Rochester, Rochester, NY 14627, USA

^dDepartment of Physics, SUNY at Buffalo, Buffalo, NY 14260-1500, USA

The production of a Higgs boson in association with a pair of $t\bar{t}$ or $b\bar{b}$ quarks plays a very important role at both the Tevatron and the Large Hadron Collider. The theoretical prediction of the corresponding cross sections has been improved by including the complete next-to-leading order QCD corrections. After a brief description of the most relevant technical aspects of the calculation, we review the results obtained for both the Tevatron and the Large Hadron Collider.

1. INTRODUCTION

The existence of a relatively light Higgs boson is both suggested by precision fits of the Standard Model (SM) and theoretically required by the Minimal Supersymmetric extension of the Standard Model (MSSM). Searches at both the Tevatron and the Large Hadron Collider (LHC) will play a crucial role in testing this hypothesis and in discriminating between different models that imply the existence of one or more Higgs bosons. In this context, the production of a Higgs boson in association with a heavy quark and antiquark pair, both $t\bar{t}$ and $b\bar{b}$, plays a very important role.

The associated production of a Higgs boson with a pair of $t\bar{t}$ quarks has a very distinctive signature, and can give the only handle on a direct measurement of the top quark Yukawa coupling, perhaps the most crucial coupling in exploring the origin of fermion masses. Observing $p\bar{p} \rightarrow t\bar{t}h$ at the Tevatron ($\sqrt{s} = 2$ TeV) will require very high luminosity [1] and will probably be beyond the machine capabilities. On the other hand, if $M_h \leq 130$ GeV, $pp \rightarrow t\bar{t}h$ is an important discovery channel for a SM-like Higgs boson at the LHC ($\sqrt{s} = 14$ TeV) [2–4]. Given the statistics expected at the LHC, $pp \rightarrow t\bar{t}h$, with $h \rightarrow b\bar{b}, \tau^+\tau^-, W^+W^-, \gamma\gamma$ will also be in-

strumental to the determination of the couplings of a discovered Higgs boson [5–9]. Several analyses show that precisions of the order of 10-15% on the measurement of the top quark Yukawa coupling can be obtained with integrated luminosities of 100 fb⁻¹ per detector. Moreover, the combined measurements of $pp \rightarrow t\bar{t}h$ with $h \rightarrow b\bar{b}$ and $h \rightarrow \tau^+\tau^-$ could provide the only model independent determination of the ratio of the bottom quark to the τ lepton Yukawa couplings [7].

The associated production of a Higgs boson with a pair of $b\bar{b}$ quarks has a very small cross section in the SM, and can therefore be used to test the hypothesis of enhanced bottom quark Yukawa couplings which is common to many extensions of the SM, such as the MSSM for large values of $\tan\beta$. Both the Tevatron and the LHC will be able to search for evidence of an enhanced $b\bar{b}h$ production, looking for a final state containing no bottom quarks (inclusive production), one bottom quark (semi-inclusive production) or two bottom quarks (exclusive production). An anomalously large inclusive Higgs boson production will be a clear signal of new physics. In the MSSM with large $\tan\beta$ this can be mainly ascribed to an enhanced bottom quark Yukawa coupling. In general, however, it cannot be uniquely interpreted, since other production channels, like the leading $gg \rightarrow h$ gluon fusion, can contribute

*Talk presented by L. Reina.

as well. Detecting one or two bottom quarks in the final state is enough to remove this ambiguity, which is the source of the interest in the semi-inclusive and exclusive production channels, in spite of their smaller cross section. The exclusive measurement corresponds to the smallest cross section, but it also has a very reduced background and this is the case we will consider in the following. The final states can be further categorized according to the decay of the Higgs boson. Existing studies have considered mostly the dominant Higgs decay channel, $h \rightarrow b\bar{b}$ [10,2], but also $h \rightarrow \mu^+\mu^-$ [11,12] and $h \rightarrow \tau^+\tau^-$ [13].

In view of their phenomenological relevance, a lot of effort has been recently invested in improving the stability of the theoretical predictions for the hadronic total cross sections for $p\bar{p}, pp \rightarrow t\bar{t}h$ and $p\bar{p}, pp \rightarrow b\bar{b}h$. Since the tree level or Leading Order (LO) cross section is affected by a very large renormalization and factorization scale dependence, the first order or Next-to-Leading Order (NLO) QCD corrections have been calculated for the inclusive $p\bar{p}, pp \rightarrow t\bar{t}h$ cross section [14–19] and for the the inclusive and exclusive $p\bar{p}, pp \rightarrow b\bar{b}h$ cross sections [20–24], while the inclusive $b\bar{b} \rightarrow h$ cross section has also recently been calculated including the Next-to-Next to Leading Order (NNLO) QCD corrections [25]. In all cases, the NLO cross section has a drastically reduced renormalization and factorization scale dependence, of the order of 15-20% as opposed to the initial 100% uncertainty of the LO cross section, and leads to increased confidence in predictions based on these results. In this proceeding we will present the results of our calculation of the NLO cross section for both the inclusive $p\bar{p}, pp \rightarrow t\bar{t}h$ [15,16,18,19] and the exclusive $p\bar{p}, pp \rightarrow b\bar{b}h$ cross sections [24], where h denotes the SM Higgs boson and, in the case of $b\bar{b}h$, also the scalar Higgs bosons of the MSSM.

The calculation of the NLO corrections to the hadronic processes $p\bar{p}, pp \rightarrow t\bar{t}h$ and $p\bar{p}, pp \rightarrow b\bar{b}h$ presents challenging technical difficulties, ranging from virtual pentagon diagrams with several massive internal and external particles to real gluon and quark emission in the presence of infrared singularities. A general overview of the techniques developed and employed in our calculation are

presented in Section 2, and the corresponding results are illustrated in Section 3 for $p\bar{p}, pp \rightarrow t\bar{t}h$ and in Section 4 for $p\bar{p}, pp \rightarrow b\bar{b}h$.

2. THE CALCULATION

The total cross section for $p\bar{p} \rightarrow Q\bar{Q}h$ (for $Q = t, b$) at $\mathcal{O}(\alpha_s^3)$ can be written as:

$$\sigma_{NLO}(p\bar{p} \rightarrow Q\bar{Q}h) = \sum_{ij} \frac{1}{1 + \delta_{ij}} \int dx_1 dx_2 \quad (1) \\ \times [\mathcal{F}_i^p(x_1, \mu) \mathcal{F}_j^{p(\bar{p})}(x_2, \mu) \hat{\sigma}_{NLO}^{ij}(\mu) + (1 \leftrightarrow 2)],$$

where $\mathcal{F}_i^{p(\bar{p})}$ are the NLO parton distribution functions (PDFs) for parton i in a (anti)proton, defined at a generic factorization scale $\mu_f = \mu$, and $\hat{\sigma}_{NLO}^{ij}$ is the $\mathcal{O}(\alpha_s^3)$ parton-level total cross section for incoming partons i and j , made of the channels $q\bar{q}, gg \rightarrow Q\bar{Q}h$ and $(q, \bar{q})g \rightarrow Q\bar{Q}h + (q, \bar{q})$, and renormalized at an arbitrary scale μ_r which we also take to be $\mu_r = \mu$. We note that the effect of varying the renormalization and factorization scales independently has been investigated and found to be negligible. The partonic center of mass energy squared, s , is given in terms of the hadronic center of mass energy squared, s_H , by $s = x_1 x_2 s_H$.

The NLO parton-level total cross section, $\hat{\sigma}_{NLO}^{ij}$, consists of the $\mathcal{O}(\alpha_s^2)$ Born cross section, $\hat{\sigma}_{LO}^{ij}$, and the $\mathcal{O}(\alpha_s)$ corrections to the Born cross section, $\delta\hat{\sigma}_{NLO}^{ij}$, including the effects of mass factorization. $\delta\hat{\sigma}_{NLO}^{ij}$ contains virtual and real corrections to the parton-level $Q\bar{Q}h$ production processes, $q\bar{q} \rightarrow Q\bar{Q}h$ and $gg \rightarrow Q\bar{Q}h$, and the tree-level $(q, \bar{q})g$ initiated processes, $(q, \bar{q})g \rightarrow Q\bar{Q}h(q, \bar{q})$, which are of the same order in α_s .

The $\mathcal{O}(\alpha_s)$ virtual and real corrections to $q\bar{q} \rightarrow Q\bar{Q}h$ and $gg \rightarrow Q\bar{Q}h$ have been discussed in detail in Refs. [16,19] and we will highlight in the following only the most challenging tasks.

2.1. Virtual corrections

The calculation of the $\mathcal{O}(\alpha_s)$ virtual corrections to $q\bar{q}, gg \rightarrow Q\bar{Q}h$ (for $Q = t, b$) proceeds by reducing each virtual diagram to a linear combination of tensor and scalar integrals, which may contain both ultraviolet (UV) and infrared (IR) divergences. Tensor integrals are further reduced

in terms of scalar integrals [26]. The finite scalar integrals are evaluated by using the method described in Ref. [27] and cross checked with the FF package [28]. The scalar integrals that exhibit UV and/or IR divergences are calculated analytically. Both the UV and IR divergences are extracted by using dimensional regularization in $d=4-2\epsilon$ dimensions. The UV divergences are then removed by introducing a suitable set of counterterms, as described in detail in Refs. [16,19,24]. The remaining IR divergences are cancelled by the analogous singularities in the soft and collinear part of the real gluon emission cross section.

The most difficult integrals arise from the IR-divergent pentagon diagrams with several massive particles. The pentagon scalar and tensor Feynman integrals originating from these diagrams present either analytical (scalar) or numerical (tensor) challenges. We have calculated the pentagon scalar integrals as linear combinations of scalar box integrals using the method of Ref. [29,30], and cross checked them using the techniques of Ref. [27]. Pentagon tensor integrals can give rise to numerical instabilities due to the dependence on inverse powers of the Gram determinant (GD), $GD = \det(p_i \cdot p_j)$ for p_i and p_j external momenta, which vanishes at the boundaries of phase space when two momenta become degenerate. These are spurious divergences, which cause serious numerical difficulties. To overcome this problem we have calculated and cross checked the pentagon tensor integrals in two ways: numerically, by isolating the numerical instabilities and extrapolating from the numerically safe to the numerically unsafe region using various techniques; and analytically, by reducing them to a numerically stable form.

2.2. Real corrections

In computing the $\mathcal{O}(\alpha_s)$ real corrections to $q\bar{q}, gg \rightarrow Q\bar{Q}h$ and $(q, \bar{q})g \rightarrow Q\bar{Q}h + (q, \bar{q})$ (for $Q=t, b$) it is crucial to isolate the IR divergent regions of phase space and extract the corresponding singularities analytically. We achieve this by using the phase space slicing (PSS) method, in both the double [31] and single [32–34] cutoff approaches. In both approaches the IR region of the $Q\bar{Q}h+g$ phase space where the emitted gluon

cannot be resolved is defined as the region where the gluon kinematic invariants:

$$s_{ig} = 2p_i \cdot p_g = 2E_i E_g (1 - \beta_i \cos \theta_{ig}) \quad (2)$$

become small. Here p_i is the momentum of an external (anti)quark or gluon (with energy E_i), $\beta_i = \sqrt{1 - m_i^2/E_i^2}$, p_g is the momentum of the radiated final state gluon (quark/antiquark) (with energy E_g), and θ_{ig} is the angle between \vec{p}_i and \vec{p}_g . In the IR region the cross section is calculated analytically and the resulting IR divergences, both soft and collinear, are cancelled, after mass factorization, against the corresponding divergences from the $\mathcal{O}(\alpha_s)$ virtual corrections.

The single cutoff PSS technique defines the IR region as that where

$$s_{ig} < s_{min} \quad , \quad (3)$$

for an arbitrarily small cutoff s_{min} . The two cutoff PSS method introduces two arbitrary parameters, δ_s and δ_c , to separately define the IR soft and IR collinear regions according to:

$$E_g < \frac{\delta_s \sqrt{s}}{2} \quad \text{soft region} \quad , \\ (1 - \cos \theta_{ig}) < \delta_c \quad \text{collinear region} \quad . \quad (4)$$

In both methods, the real contribution to the NLO cross section is computed analytically below the cutoffs and numerically above the cutoffs, and the final result is independent of these arbitrary parameters. With this respect, it is crucial to study the behavior of σ_{NLO} in a region where the cutoff(s) are small enough to justify the analytical calculations of the IR divergent contributions to the real cross section, but not so small as to cause numerical instabilities.

3. RESULTS FOR $t\bar{t}h$ PRODUCTION

The impact of NLO QCD corrections on the tree level cross section for $pp \rightarrow t\bar{t}h$ (LHC) production in the SM is illustrated in Figs. 1 and 2. Similar results for the case of $p\bar{p} \rightarrow t\bar{t}h$ (Tevatron) can be found in Ref. [15,16]. Results for σ_{LO} are obtained using the 1-loop evolution of $\alpha_s(\mu)$ and CTEQ5L parton distribution functions [35], while results for σ_{NLO} are obtained using the 2-loop evolution of $\alpha_s(\mu)$ and CTEQ5M parton distribution functions, with $\alpha_s^{NLO}(M_Z)=0.118$. The

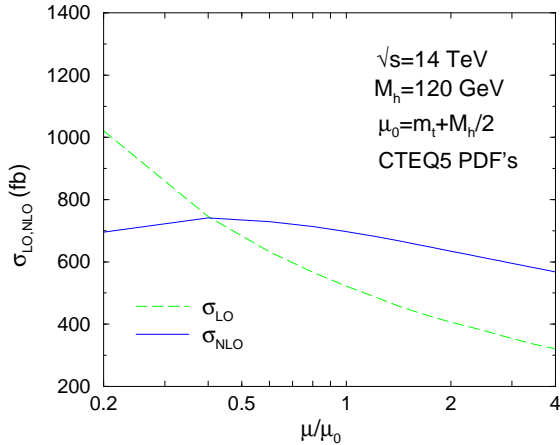


Figure 1. Dependence of $\sigma_{LO,NLO}(pp \rightarrow t\bar{t}h)$ on the renormalization/factorization scale μ , at $\sqrt{s_H}=14$ TeV, for $M_h=120$ GeV.

top quark mass is renormalized in the OS scheme and its pole mass is fixed at $m_t=174$ GeV.

Fig. 1 illustrates the renormalization/factorization scale dependence of σ_{LO} and σ_{NLO} at the LHC. The NLO cross section shows a drastic reduction of the scale dependence with respect to the lowest order prediction. Fig. 2 complements this information by illustrating the dependence of the LO and NLO cross sections on the Higgs boson mass at the LHC. For scales $\mu \geq 0.4\mu_0$ ($\mu_0 = m_t + M_h/2$) the NLO corrections enhance the cross section. We estimate the remaining theoretical uncertainty on the NLO result to be of the order of 15-20%, due to the left over μ -dependence, the error from the PDFs, and the the error on the top quark pole mass m_t .

4. RESULTS FOR $b\bar{b}h$ PRODUCTION

We evaluate the fully exclusive cross section for $b\bar{b}h$ production by requiring that the transverse momentum of both final state bottom and anti-bottom quarks be larger than 20 GeV ($p_T^b > 20$ GeV), and that their pseudorapidity satisfy the condition $|\eta_b| < 2$ for the Tevatron and $|\eta_b| < 2.5$ for the LHC. This corresponds to an experiment measuring the Higgs decay products along with two high p_T bottom quark jets. In order to better simulate the detector response, the final state

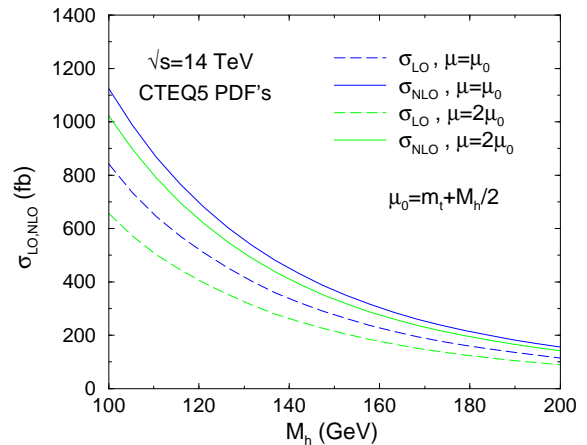


Figure 2. $\sigma_{NLO}(pp \rightarrow t\bar{t}h)$ and $\sigma_{LO}(pp \rightarrow t\bar{t}h)$ as functions of M_h , at $\sqrt{s_H}=14$ TeV, for $\mu = m_t + M_h/2$ and $\mu = 2m_t + M_h$.

gluon and the bottom/anti-bottom quarks are treated as distinct particles only if the separation in the azimuthal angle-pseudorapidity plane is $\Delta R > 0.4$. For smaller values of ΔR , the four momentum vectors of the two particles are combined into an effective bottom/anti-bottom quark momentum four-vector.

As for $t\bar{t}h$ production, our numerical results for the NLO (LO) cross sections are obtained using CTEQ5M (CTEQ5L) PDFs [35] and the 2-loop (1-loop) evolution of $\alpha_s(\mu)$. In the $b\bar{b}h$ case, however, we have also investigated the dependence of the NLO result on the choice of the renormalization scheme for the bottom quark Yukawa coupling. The strong scale dependence of the \overline{MS} bottom quark mass ($\overline{m}_b(\mu)$) plays a special role in the perturbative evaluation of the $b\bar{b}h$ production cross section since it enters in the overall bottom quark Yukawa coupling. The same is not true for $t\bar{t}h$ production since the \overline{MS} top quark mass has only a very mild scale dependence. The bottom quark pole mass is taken to be $m_b = 4.6$ GeV. In the OS scheme the bottom quark Yukawa coupling is calculated as $g_{b\bar{b}h} = m_b/v$, while in the \overline{MS} scheme as $g_{b\bar{b}h}(\mu) = \overline{m}_b(\mu)/v$, where we use the 2-loop (1-loop) \overline{MS} bottom quark mass for the NLO (LO) cross section respectively.

The impact of NLO QCD corrections on the tree level cross section for $b\bar{b}h$ exclusive produc-

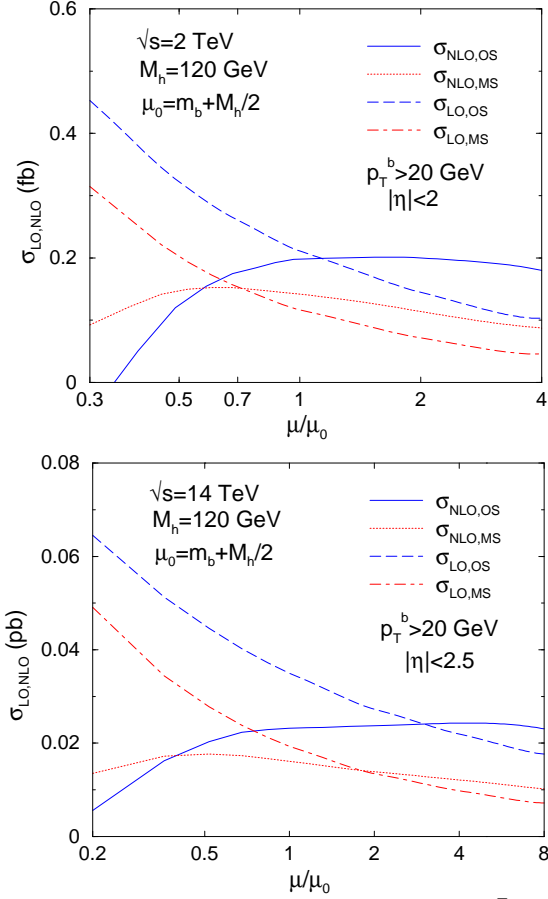


Figure 3. σ_{NLO} and σ_{LO} for $p\bar{p} \rightarrow b\bar{b}h$ at $\sqrt{s} = 2$ TeV (top) and for $pp \rightarrow b\bar{b}h$ at $\sqrt{s} = 14$ TeV (bottom) as a function of the renormalization/factorization scale μ , for $M_h = 120$ GeV.

tion in the SM is summarized in Fig. 3 for both the Tevatron and the LHC. In both the OS and the \overline{MS} schemes the stability of the cross section is greatly improved at NLO, and the correspondent theoretical uncertainty reduced to 15-20%. The \overline{MS} results seem to have overall a better perturbative behavior, although the variation of the NLO cross section about its point of least sensitivity to the renormalization/factorization scale is almost the same when one uses the OS or \overline{MS} schemes for the bottom Yukawa coupling. This indicates that the running of the Yukawa coupling is not the only important factor to determine the overall perturbative stability of the cross section.

The difference between the OS and \overline{MS} results at their plateau values should probably be interpreted as an additional theoretical uncertainty.

Finally, in Fig. 4 we illustrate the dependence of the exclusive cross section, at the Tevatron and at the LHC, on the Higgs boson mass, both in the SM and in some scenarios of the MSSM, corresponding to $\tan\beta = 10, 20$ and 40 . For the Tevatron we consider the case of the light MSSM scalar Higgs boson (h^0) while for the LHC we consider the case of the heavy MSSM scalar Higgs boson (H^0). We see that the rate for $b\bar{b}h$ production can be significantly enhanced in a supersymmetric model with large values of $\tan\beta$, and makes $b\bar{b}h$ a very important mode for discovery of new physics at both the Tevatron and the LHC.

Acknowledgments

The work of S.D. (C.J., L.H.O., L.R.) is supported in part by the U.S. Department of Energy under grant DE-AC02-98CH10886 (DE-FG02-97ER41022, DE-FG-02-91ER40685, DE-FG02-97ER41022). The work of D.W. is supported in part by the National Science Foundation under grant No. PHY-0244875.

REFERENCES

1. J. Goldstein *et al.*, Phys. Rev. Lett. **86**, 1694 (2001), hep-ph/0006311.
2. ATLAS Collaboration (1999), Technical Design Report, Vol. II, CERN/LHCC/99-15.
3. M. Beneke *et al.* (2000), hep-ph/0003033.
4. V. Drollinger, T. Muller, and D. Denegri (2001), hep-ph/0111312.
5. D. Zeppenfeld, R. Kinnunen, A. Nikitenko, and E. Richter-Was, Phys. Rev. **D62**, 013009 (2000), hep-ph/0002036.
6. D. Zeppenfeld (2002), hep-ph/0203123.
7. A. Belyaev and L. Reina, JHEP **08**, 041 (2002), hep-ph/0205270.
8. F. Maltoni, D. Rainwater, and S. Willenbrock, Phys. Rev. **D66**, 034022 (2002), hep-ph/0202205.
9. M. Dürssen (2003), ATL/PHYS-2003-30.
10. M. Carena *et al.*, Report of the Tevatron Higgs working group (2000), hep-ph/0010338.

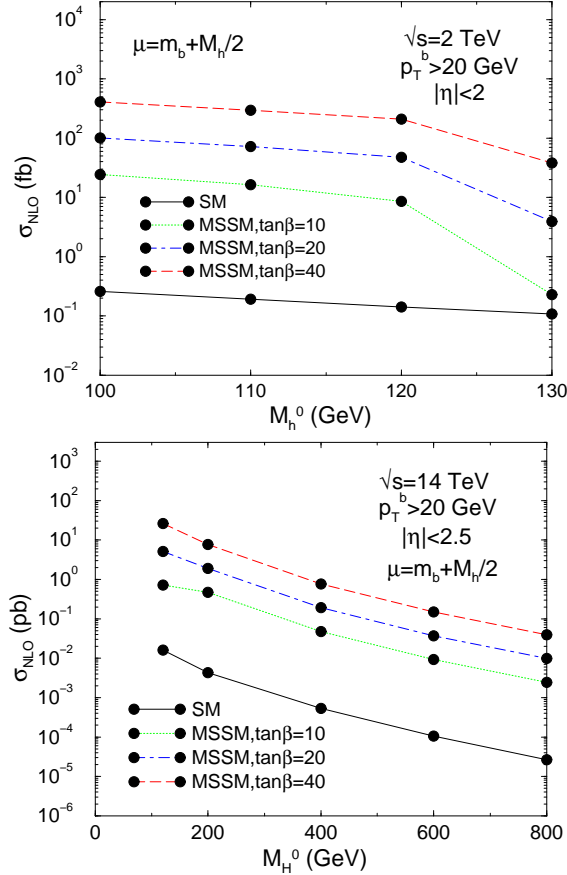


Figure 4. $\sigma_{NLO,MS}$ for $p\bar{p} \rightarrow b\bar{b}h$ production at $\sqrt{s} = 2$ TeV (top) and $pp \rightarrow b\bar{b}h$ production at $\sqrt{s} = 14$ TeV (bottom) in the SM and in the MSSM with $\tan\beta = 10, 20$, and 40 .

11. S. Dawson, D. Dicus, and C. Kao, Phys. Lett. **B545**, 132 (2002), hep-ph/0208063.
12. E. Boos, A. Djouadi, and A. Nikitenko (2003), hep-ph/0307079.
13. E. Richter-Was *et al.*, Int. J. Mod. Phys. **A13**, 1371 (1998).
14. W. Beenakker, S. Dittmaier, M. Krämer, B. Plümper, M. Spira, and P. Zerwas, Phys. Rev. Lett. **87**, 201805 (2001), hep-ph/0107081.
15. L. Reina and S. Dawson, Phys. Rev. Lett. **87**, 201804 (2001), hep-ph/0107101.
16. L. Reina, S. Dawson, and D. Wackeroth, Phys. Rev. **D65**, 053017 (2002), hep-ph/0109066.
17. W. Beenakker, S. Dittmaier, M. Krämer, B. Plümper, M. Spira, and P. Zerwas, Nucl. Phys. **B653**, 151 (2003), hep-ph/0211352.
18. S. Dawson, L. H. Orr, L. Reina, and D. Wackeroth, Phys. Rev. **D67**, 071503 (2003), hep-ph/0211438.
19. S. Dawson, C. Jackson, L. H. Orr, L. Reina, and D. Wackeroth, Phys. Rev. **D68**, 034022 (2003), hep-ph/0305087.
20. D. Dicus, T. Stelzer, Z. Sullivan, and S. Willenbrock, Phys. Rev. **D59**, 094016 (1999), hep-ph/9811492.
21. C. Balazs, H.-J. He, and C. P. Yuan, Phys. Rev. **D60**, 114001 (1999), hep-ph/9812263.
22. J. Campbell, R. K. Ellis, F. Maltoni, and S. Willenbrock, Phys. Rev. **D67**, 095002 (2003), hep-ph/0204093.
23. S. Dittmaier, M. Krämer, and M. Spira (2003), hep-ph/0309204.
24. S. Dawson, C. Jackson, L. Reina, and D. Wackeroth (2003), hep-ph/0311067.
25. R. V. Harlander and W. B. Kilgore, Phys. Rev. **D68**, 013001 (2003), hep-ph/0304035.
26. G. Passarino and M. J. G. Veltman, Nucl. Phys. **B160**, 151 (1979).
27. A. Denner, Fortsch. Phys. **41**, 307 (1993).
28. G. J. van Oldenborgh and J. A. M. Vermaseren, Z. Phys. **C46**, 425 (1990).
29. Z. Bern, L. J. Dixon, and D. A. Kosower, Phys. Lett. **B302**, 299 (1993), erratum-ibid. **B318**, 649 (1993), hep-ph/9212308.
30. Z. Bern, L. J. Dixon, and D. A. Kosower, Nucl. Phys. **B412**, 751 (1994), hep-ph/9306240.
31. B. W. Harris and J. F. Owens, Phys. Rev. **D65**, 094032 (2002), hep-ph/0102128.
32. W. T. Giele and E. W. N. Glover, Phys. Rev. **D46**, 1980 (1992).
33. W. T. Giele, E. W. N. Glover, and D. A. Kosower, Nucl. Phys. **B403**, 633 (1993), hep-ph/9302225.
34. S. Keller and E. Laenen, Phys. Rev. **D59**, 114004 (1999), hep-ph/9812415.
35. H. L. Lai *et al.* (CTEQ), Eur. Phys. J. **C12**, 375 (2000), hep-ph/9903282.